International Journal of Pharmaceutics 361 (2008) 177–188

Contents lists available at ScienceDirect

International Journal of Pharmaceutics

journal homepage: www.elsevier.com/locate/ijpharm

Pharmaceutical Nanotechnology

High bioavailability from nebulized itraconazole nanoparticle dispersions with biocompatible stabilizers

Wei Yang[a], Jasmine Tam[b], Dave A. Miller[a,1], Jiping Zhou[c], Jason T. McConville[a], Keith P. Johnston[b,**], Robert O. Williams III[a,*]

[a] College of Pharmacy, The University of Texas at Austin, 1 University Station, Mail Stop A1920, Austin, TX 78712, USA
[b] Department of Chemical Engineering, The University of Texas at Austin, 1 University Station, Mail Stop C0400, Austin, TX 78712, USA
[c] Texas Materials Institute, The University of Texas at Austin, Austin, TX 78712, USA

ARTICLE INFO

Article history:
Received 2 March 2008
Received in revised form 5 May 2008
Accepted 6 May 2008
Available online 14 May 2008

Keywords:
Poorly water-soluble drug
Amorphous
Solid solution
Bioavailability
Antifungal
Aspergillosis

ABSTRACT

A nebulized dispersion of amorphous, high surface area, nanostructured aggregates of itraconazole (ITZ):mannitol:lecithin (1:0.5:0.2, w/w) yielded improved bioavailability in mice. The ultra-rapid freezing (URF) technique used to produce the nanoparticles was found to molecularly disperse the ITZ with the excipients as a solid solution. Upon addition to water, ITZ formed a colloidal dispersion suitable for nebulization, which demonstrated optimal aerodynamic properties for deep lung delivery and high lung and systemic levels when dosed to mice. The ITZ nanoparticles produced supersaturation levels 27 times the crystalline solubility upon dissolution in simulated lung fluid. A dissolution/permeation model indicated that the absorption of 3 μm ITZ particles is limited by the dissolution rate (BCS Class II behavior), while absorption is permeation-limited for more rapidly dissolving 230 nm particles. The predicted absorption half-life for 230 nm amorphous ITZ particles was only 15 min, as a result of the small particle size and high supersaturation, in general agreement with the *in vivo* results. Thus, bioavailability may be enhanced, by decreasing the particle size to accelerate dissolution and increasing permeation with (1) an amorphous morphology to raise the drug solubility, and (2) permeability enhancers.

1. Introduction

Improving the bioavailability of active pharmaceutical ingredients (API), defined as the rate and extent of the API that reaches systemic circulation is a major goal of pharmaceutical drug delivery. Enhancements in bioavailability may increase patient compliance. The effectiveness of poorly water-soluble APIs can be severely limited when solubilities are too low to produce systemic therapeutic levels. Several strategies have been developed to improve the aqueous dissolution properties of poorly water-soluble API formulations, including the use of surfactants, emulsification processes, solution based precipitation and solid state manipulation (Betageri and Makarla, 1995; Mawson et al., 1997; Rogers et al., 2001; Sarkari et al., 2002; Hu et al., 2004; Matteucci et al., 2007). Amorphous particles may be designed to produce high levels of supersaturation relative to the solubility of the crystalline state (Hancock and Parks, 2000). Cryogenic technologies have been used to produce highly porous, amorphous, nanostructured particles with improved dissolution rates and high supersaturation drug levels relative to the solubility of the crystalline state for poorly water-soluble APIs (Vaughn et al., 2005; McConville et al., 2006; Overhoff et al., 2007a). The Spray Freezing into Liquid (SFL) process forms a solid dispersion or solid solution composed of drug domains within a polymer matrix by spraying the drug/excipients solution directly into liquid nitrogen (Vaughn et al., 2005). The URF particle engineering process utilizes rapid freezing of a drug/excipient solution onto a cryogenic substrate of desired thermal conductivity to obtain a solid dispersion/solution (Overhoff et al., 2007a).

ITZ, a broad-spectrum antimycotic triazole has been used for both prophylaxis and treatment of invasive fungal diseases for the last two decades. ITZ is a poorly soluble weak base with a calculated log *P* of 6.2. Its aqueous solubility is estimated at approximately 1 ng/mL at neutral pH and approximately 4 μg/mL at pH 1 (Peeters et al., 2002). Given the high log *P* value, ITZ is classified as a class II drug according to the Biopharmaceutical Classification System (BCS) (Amidon et al., 1995). Sporanox® oral capsule and solution, ITZ preparations for oral administration on the market, show low oral absorption and considerably varied pharmacokinetics in

* Corresponding author. Tel.: +1 512 471 4681; fax: +1 512 471 7474.
** Corresponding author. Tel.: +1 512 471 4617; fax: +1 512 471 7060.
E-mail addresses: kpj@che.utexas.edu (K.P. Johnston), williro@mail.utexas.edu (R.O. Williams III).
[1] Current address: Hoffmann-La Roche Inc., Pharmaceutical & Analytical Research & Development, 340 Kingsland St., Nutley, NJ 07110-1199, USA.

0378-5173/$ – see front matter © 2008 Elsevier B.V. All rights reserved.
doi:10.1016/j.ijpharm.2008.05.003

immunocompromised patients (Smith et al., 1992; Barone et al., 1993; Poirier et al., 1997). To treat invasive fungal infection, especially *Aspergillus* spp. infections in immunocompromised patients, ITZ levels of greater than 0.5 μg/g of lung tissue, or 0.5 μg/mL of blood (Sobel, 2000) is generally required.

The design of rapidly dissolving drug nanoparticles offers potential improvements in therapeutic efficacy, stability, patient compliance, and safety (Ebbesen and Jensen, 2006; Yang et al., 2008). The route of administration is as important as the drug formulation for achieving therapeutic success (Lin et al., 2001; Mehrad et al., 2001; Clark and Hajjeh, 2002; Singh and Husain, 2003). Pulmonary delivery of a wide spectrum of drug substances, including proteins/peptides, nucleic acids, and antibiotics to the lungs can be highly effective for localized treatment or prophylaxis of pulmonary diseases, including lung infections, cystic fibrosis, and asthma (Edwards and Dunbar, 2002). Pulmonary delivery is a non-invasive route that facilitates deposition of large drug doses to the lungs, and offers the potential for high systemic absorption. Efficient systemic absorption is attributed to the lung's large absorptive surface area, very thin diffusion path to the blood stream, elevated blood flow, relatively low metabolic activity and the avoidance of hepatic first pass metabolism (Adje and Gupta, 1997). Particle size distribution and morphology have pronounced effects on all aspects of pulmonary drug delivery, including deposition in the respiratory tract, dissolution in the lung lining fluid and the clearance mechanism (Chow et al., 2007). The particle size of aerosols is determined by the inhalation device and physicochemical properties of the drug formulation, such as viscosity and surface tension (Mccallion et al., 1995).

Pulmonary drug delivery targeted to the alveoli is advantageous and critical for systemic absorption (Courrier et al., 2002). The concept of improving bioavailability of poorly water-soluble APIs by pulmonary delivery of nanostructured aggregates has been recently reported in mouse models. Inhalation of a nebulized ITZ nanoparticle composition (ITZ:polysorbate 80:poloxamer 407 = 1:0.75:0.75 by weight ratio, prepared by SFL; namely SFL-ITZ) by mice for 20 min produced relatively high drug concentrations in lung tissue and about one-third the drug level in systemic circulation compared to Sporanox® solution administered orally at the same dose (Vaughn et al., 2006). Nebulization of aqueous colloidal dispersions of amorphous cyclosporin A/polysorbate 80 nanoparticles into mice produced therapeutic lung levels and systemic concentrations below toxic limits (Tam et al., 2008).

Inclusion of certain surface active excipients in pulmonary formulations may enhance bioavailability, but may also interfere with cell lipid bilayer membranes and thus raise long term safety concerns (Patton et al., 1989). The objective of this study was to develop an ITZ nanoparticle dispersion for pulmonary delivery by nebulization that does not require the use of synthetic polymers and surfactants to achieve high supersaturation values *in vitro* and high bioavailability. Mannitol is a widely used excipient approved by the Food and Drug Administration (FDA) for inhalation purposes (Bosquillon et al., 2001, http://www.accessdata.fda.gov/scripts/cder/iig/getiigWEB.cfm). Lecithin, currently FDA approved for pulmonary formulations, contains mainly dipalmitoylphosphatidylcholine (DPPC), the primary component of endogenous human lung surfactant (Goerke, 1998). We hypothesize that a high surface area nanostructured ITZ composition encompassing soluble, and/or biodegradable, and/or biocompatible materials such as mannitol and lecithin, ITZ:mannitol:lecithin = 1:0.5:0.2 (by weight ratio, namely URF-ITZ), can be inhaled by nebulization to produce high supersaturation levels rapidly in the alveolar fluid. Pulmonary delivery of the nanostructured ITZ composition may provide not only local lung deposition, but possibly high systemic bioavailability with low toxicity.

The URF-ITZ dry powder and its aqueous dispersion suitable for nebulization were characterized by a wide variety of techniques. A single-dose 24-h pharmacokinetic study was also performed in mice to assess the bioavailability of nebulized URF-ITZ nanoparticle dispersion by inhalation and to explore the factors influencing the pharmacokinetic parameters. In order to better understand how particle size and solubility (supersaturation) may be designed to enhance absorption rates in the alveoli, a recently developed model of Tam et al. (2008) was used to analyze the individual effects of dissolution.

2. Materials and methods

2.1. Materials

The following materials were purchased: ITZ, micronized pharmacopeial grade (Hawkins Chemical, Minneapolis, MN); mannitol and polysorbate 80 (Spectrum Chemicals, Gardena, CA); lecithin, 1,4-dioxane (Fisher Scientific, Fair Lawn, NJ); diethanolamine (VWR International, West Chester, PA); acetonitrile (EM Industries Inc., Gibbstown, NJ). All organic solvents used were HPLC grade. Other reagents used were at least ACS grade.

2.2. Preparation of nanostructured aggregate powder of ITZ using URF technology

For a standard batch of the formulation, lecithin (118 mg) was dissolved in a mixture of 1,4-dioxane and purified water (65/35, v/v) co-solvent system (200 mL) using a magnetic stirrer. ITZ (588 mg) and mannitol (294 mg) were subsequently dissolved in the mixture, this provided a dissolved solids ratio of ITZ:mannitol:lecithin of 1:0.5:0.2 by weight. The solution was frozen using the URF apparatus (Evans et al., 2006; Overhoff et al., 2007a). Briefly, the solution was applied to the cryogenic solid substrate (which was previously cooled to −70 °C), whereby the solution was frozen rapidly. The resultant frozen solids were collected and lyophilized using a VirTis Advantage bench top tray lyophilizer (The VirTis Company, Inc., Gardiner, NY, USA). The dry powder was stored in a desiccator under vacuum at room temperature.

2.3. Preparation of physical mixture

A physical mixture consisting of ITZ:mannitol:lecithin in the weight ratio of 1:0.5:0.2 was mixed by geometric dilution and trituration using a ceramic mortar and pestle.

2.4. Powder X-ray diffraction (XRD)

The URF-ITZ powder, the physical mixture, the bulk ITZ and mannitol were examined by wide angle XRD. A Philips 1710 X-ray diffractometer with a copper target (CuKa1, λ = 1.54056 Å) and nickel filter (Philips Electronic Instruments Inc., Mahwah, NJ) was used to obtain the XRD patterns. The voltage was 40 kV and the current was 40 mA. Samples were analyzed in the 2-theta range from 10 to 50° using a step size of 0.05 2-theta degree with a dwell time of 2 s.

2.5. Scanning electron microscopy (SEM)

SEM was used to evaluate the morphology of the samples. The samples were mounted onto an aluminum stage using conductive carbon tape. Samples were coated using a model K575 sputter coater (Emitech Products, Inc., Houston, TX) with gold/palladium for 20 s in a high vacuum evaporator. SEM was performed using a Hitachi S-4500 field emission scanning electron microscope

(Hitachi High-Technologies Corp., Tokyo, Japan) operating at an accelerating voltage of 10–15 kV. Images were captured with Quartz PCI software (Quartz Imaging Corporation, Vancouver, BC, Canada).

2.6. Scanning transmission electron microscopy (STEM)

The URF-ITZ powder was further characterized using STEM, by placing the dry powder on a Holey Carbon Support Film with 200 Mesh Copper Grids (Jed Pella, Inc., Redding, CA) and viewing on a JEOL 2010F transmission electron microscope (JEOL USA, Inc., Peabody, MA) equipped with an energy dispersive spectroscopy (EDS) detector for elemental characterization.

2.7. Thermal analysis

Differential Scanning Calorimetry (DSC) of the URF-ITZ powder and each component was conducted using modulated temperature DSC (MTDSC), Model 2920 (TA Instruments, New Castle, DE), equipped with a refrigerated cooling system. Dry nitrogen gas was used as the purge gas through the DSC cell at a flow rate of 40 mL/min. Samples were weighed to 10–15 mg in aluminum crimped pans, Kit 0219-0041 (PerkinElmer Instruments, Norwalk, CT). The mass of the empty sample pan was matched with that of the empty reference pan within ±0.2 mg. Samples were heated at a ramp rate of 10 °C/min from −30 to 200 °C with a modulation temperature amplitude of 1 °C/60 s for all studies. Data was analyzed using TA Universal Analysis 2000 software (TA Instruments, New Castle, DE). Amorphous pure ITZ was prepared by the URF process as described above. Amorphous mannitol and lecithin were prepared by quench-cooling (Kim et al., 1998). In brief, accurately weighed mannitol and lecithin powders were heated to 200 and 150 °C, respectively, in sealed aluminum DSC pans, the temperature was held for 15 min. The samples were then quench-cooled in liquid nitrogen externally to the DSC instrument. DSC was conducted by placing back the samples to pre-cooled sample chamber (−50 °C), and thermograms were recorded the same as with the other samples.

2.8. True density measurements

True density of ITZ, mannitol and lecithin was measured using an AccuPyc 1330 helium pycnometer (Micrometrics; Norcross, GA). The samples were dried overnight. Upon measurement, the samples were purged 20 times with dry helium at 19.85 psi followed by six analytical runs at 19.85 psi. The equilibration rate was 0.0050 psi/min. Measurements were performed in triplicate.

2.9. Particle size analysis by laser diffraction

Particle size distribution, based on volume fraction, of the URF-ITZ powder, the physical mixture and bulk ITZ was measured by laser diffraction with a Malvern Mastersizer-S (Malvern Instruments, Ltd., Worcestershire, UK). To measure the particle size distribution, powder aliquots were dispersed in 5 mL purified water, sonicated, and the dispersions were added to the sample reservoir to produce light obscuration in the range of 10–15%. Bulk ITZ was dispersed in 5 mL of a 0.1% polysorbate 80 aqueous solution for pre-wetting due to its high hydrophobicity. Sonication was used during the measurement to break up the agglomerated particles. Values reported are the average of at least three determinations.

2.10. Brunauer–Emmett–Teller (BET) specific surface area analysis

Specific surface area was measured using a Nova 2000 version 6.11 instrument (Quantachrome Instruments, Boynton Beach, FL). An aliquot of powder was added to a 12-mm Quantachrome bulb sample cell and degassed overnight prior to analysis. The data was then analyzed using NOVA Enhanced Data Reduction Software (version 2.13).

2.11. Dissolution testing at supersaturation conditions

Dissolution testing at supersaturated conditions was conducted in a USP 25 dissolution apparatus model Vankel 7000 Dissolution Tester (Vankel Technology Group, Cary, NC) using 100 mL glass dissolution vessels and stirred with small paddles at 100 rpm. Simulated lung fluid containing 0.02% DPPC (Davies and Feddah, 2003; Cook et al., 2005) at 37 °C was used as the dissolution medium. An equivalent of 100 μg ITZ in a colloidal dispersion (equal to 100-times of equilibrium solubility of crystalline ITZ (C_{eq})) at 4 °C was added to the dissolution vessels ($n = 6$) within one second immediately after sonication. Aliquots of 2 mL of the dissolution media were taken at 5, 15, 30, 60, 120 and 180 min. All samples were filtered through a 0.2 μm GHP Acrodisc filter (Pall Corporation, East Hills, NY), and diluted with acetonitrile for content analysis. The ITZ content was determined using a Shimadzu LC-10A high performance liquid chromatography (HPLC) system (Shimadzu Corporation, Columbia, MD) equipped with an Alltech Inertsil™ ODS-2 5 μm, 150 mm × 4.6 mm, C-18 column (Alltech Associates, Inc., Deerfield, IL). The mobile phase was acetonitrile:water:diethanolamine (70:30:0.05) and it eluted the ITZ peak at approximately 5.5 min at 25 °C with a flow rate of 1 mL/min. The ITZ absorbance was measured at a wavelength λ_{max} of 263 nm.

2.12. In vitro aerosol performance

A colloidal dispersion of the URF-ITZ powder was prepared for nebulization by dispersing the powder in purified water (equivalent to 20 mg/mL ITZ) using ultrasonication in an ice bath. An aliquot (5 mL) of the dispersion was nebulized using an Aeroneb® Professional micropump nebulizer (Nektar Inc., Mountain View, CA) for 10 min at an air flow rate of 28.3 L/min. The flow rate was maintained by a vacuum pump (MFG Corp., Benton Harbor, MI) and calibrated by a TSI mass flow meter, Model 4000 (TSI Inc., St. Paul, MN). The *in vitro* deposition characteristics of the colloidal dispersion of URF-ITZ for nebulization, was investigated using an eight-stage Andersen cascade impactor (Thermo-Electron Corp., Symrna, GA). The cascade impactor was assembled and operated in accordance with USP General Chapter 601 to assess the drug delivered. After deposition onto the stages of the impactor, the mass deposited on each of the stages was collected and the total mass of drug on each stage was analyzed by HPLC. The aerosolization behavior was described in terms of total emitted dose (TED), mass median aerodynamic diameter (MMAD), geometric standard deviation (GSD), and percentage fine particle fraction (FPF; defined as the percentage of droplets with an aerodynamic diameter less than 4.7 μm).

2.13. Stability study

The URF-ITZ powder was stored in desiccators under vacuum at room temperature, and the physical stability was assessed by XRD at 1, 3 and 12 months.

The physical stability of the colloidal dispersion of URF-ITZ for nebulization was also investigated. The colloidal dispersion of

URF-ITZ for nebulization was prepared as previously described. It was allowed to equilibrate at 25 °C for 15 min, and then was quench frozen using excess liquid nitrogen. The colloidal dispersion was lyophilized, and the resultant powder was investigated by XRD.

2.14. In vivo pulmonary dosing of mice

Fourteen male ICR mice (Harlan Sprague Dawley, Inc., Indianapolis, IN) were dosed by inhalation of the nebulized colloidal dispersion of the URF-ITZ (equivalent to 20 mg/mL ITZ) for 10 min in a whole-body dosing chamber as previously described (McConville et al., 2005). This restraint-free chamber was designed to hold up to 14 mice. An Aeroneb Professional micropump nebulizer was situated at the inlet of the chamber, and the colloidal dispersion of the URF-ITZ was nebulized through the inlet into the chamber with an air flow rate of 1 L/min. Following exposure to the aerosol cloud, the mice were sacrificed by carbon dioxide asphyxiation at 0.5, 1, 2, 4, 6, 10, and 24 h time points post-dosing. Blood samples were taken by cardiac puncture, and the lungs were harvested. The study protocol was approved and conducted in accordance with the Institutional Animal Care and Use Committee (IACUC) guidelines at The University of Texas at Austin.

2.15. Plasma and lung analysis

Serum was separated by centrifugation at 3000 × *g* for 10 min in a 1.5 mL micro-centrifuge tube using a Microfuge® 18 centrifuge (Beckman Coulter, Fullerton, CA). The serum and lung samples were stored at −20 °C until analyzed. The homogenized lung samples were prepared by adding 1 mL of normal saline to each of the harvested lung and homogenized using tip sonication on an ice bath. Drug levels in the calibration standards, serum and homogenized lung samples were analyzed as previously indicated (Vaughn et al., 2006). Briefly, to an aliquot of 250 μL serum or 250 μL of lung homogenate, 50 μL of 0.3 N barium hydroxide and 50 μL of 0.4 N zinc sulfate heptahydrate solutions were added and vortex mixed for 30 s to precipitate water-soluble proteins. Acetonitrile (1 mL) containing 500 ng/mL ketoconazole as an internal reference standard was added to each sample followed by vortex mixing for 1.5 min. Each sample was then centrifuged at 3000 × *g* for 15 min. The supernatant was transferred to a clean 1.5 mL micro-centrifuge tube and dried under a stream of nitrogen gas. Each sample was reconstituted with 250 μL mobile phase (62% acetonitrile: 38% 0.05 M potassium phosphate monobasic buffer adjusted to pH 6.7 with NaOH) and analyzed by HPLC with an Alltech Inertsil™ ODS-2 5 μm, 250 mm × 4.6 mm, C-18 column protected by a C-18 guard column (5 μm, 7.5 mm × 4.6 mm) (Alltech Associates, Inc., Deerfield, IL). The injection volume was 100 μL, and the wavelength of absorption was 263 nm (λ_{max}). The limit of detection and quantitation for ITZ was 10 and 30 ng/mL, respectively. The column was maintained at 37 °C during the analysis. The ITZ peak eluted at approximately 18 min and the ketoconazole peak eluted at 9.3 min at a mobile phase flow rate of 1.0 mL/min.

2.16. Pharmacokinetic analysis

Pharmacokinetic parameters for lung and serum were derived by non-compartmental and one-compartmental analysis, respectively. Pharmacokinetic parameters were estimated by standard methods. C_{max} was the maximal concentration observed, T_{max} was the time to C_{max}, and they were obtained from the individual concentration–time curves. The $K_{01\ absorption}$ and $K_{10\ elimination}$ rate constants were determined by linear regression of the points of the log–linear plasma concentration versus time curve. The area under the concentration–time curve from time zero to infinity ($AUC_{0-\infty}$) was determined by use of the linear trapezoidal rule with extrapolation to infinity by using the $K_{10\ elimination}$ rate constant. The $t_{1/2}$ was defined as 0.693/rate constant K (Rowland and Tozer, 1995).

3. Results

3.1. Physicochemical properties of URF–ITZ powder

The URF process was employed to make the nanostructured aggregate powder with an ITZ potency of 56%. ITZ is a highly crystalline hydrophobic molecule with a molecular weight of 705.64. The degree of crystallinity in the ITZ/excipient mixture has been shown to affect the solubility and dissolution rate of ITZ in the mixture (Vaughn et al., 2005). The crystallinity of bulk ITZ, mannitol, URF-ITZ and the physical mixture were examined by XRD and the profiles are depicted in Fig. 1. The characteristic crystalline peaks for ITZ were found at 14.5, 17.6, 20.3, and 23.45 2-theta degrees, as seen in the bulk ITZ (purchased from the manufacturer) and physical mixture samples. The physical mixture of ITZ:mannitol:lecithin (1:0.5:0.2 ratio by weight) showed a qualitative reduction in crystalline intensity for both ITZ and mannitol. The URF-ITZ powder was amorphous as indicated by the absence of the characteristic crystalline peaks of ITZ and mannitol.

From the SEM images, the bulk ITZ and the physical mixture were composed of large, compact crystals at the micron-scale, ranging up to about 5 μm in length (Fig. 2a and b). In contrast, a highly porous structure with more regularly shaped particles of the URF-ITZ powder was observed at higher magnifications in Fig. 2c and d, displaying aggregated nanoparticles that formed a porous matrix. Closer inspection of the morphology by STEM demonstrated that the bridged, round shaped primary particles of the nanostructured aggregates were about 30–50 nm in diameter, as seen in Fig. 3a.

3.2. Energy dispersive spectroscopy (EDS)—elemental characterization

The ITZ molecule ($C_{35}H_{38}Cl_2N_8O_4$) may be distinguished from other molecules present in the formulation due to the presence of two chlorine atoms; whereas mannitol contains only carbon, oxygen and hydrogen, and lecithin also contains phosphorus. Chlorine may be used as a marker to determine the distribution of ITZ molecules within the nanostructured aggregates. EDS was used to map the compositional distribution of the elements, including: carbon, oxygen and chlorine.

Elemental distribution mapping for carbon, oxygen and chlorine contained in the nanoparticle aggregates of URF-ITZ scanned by EDS are presented in Fig. 3c–e along with a STEM image of the scanned nanostructured aggregates in Fig. 3b. Element distribution images showed colored dots, representing the presence of a particular chemical element, in contrast to the black background. It can be seen that the distribution of each element is consistent with the shape and density of the aggregated nanoparticles scanned, including the presence of the pores.

3.3. Thermal analysis

MTDSC was carried out to study the thermal properties of the URF-ITZ powder and its individual components. The glass transition temperature (T_g) of URF pure ITZ (no excipients; 100% potency), quench-cooled mannitol and quench-cooled lecithin were 59.6 °C (consistent with reports of Six et al., 2001 and Verreck et al., 2003), 16.8 and 5.1 °C, respectively, as shown in Fig. 4 thermograms. The URF-ITZ powder (ITZ:mannitol:lecithin = 1:0.5:0.2 ratio by weight)

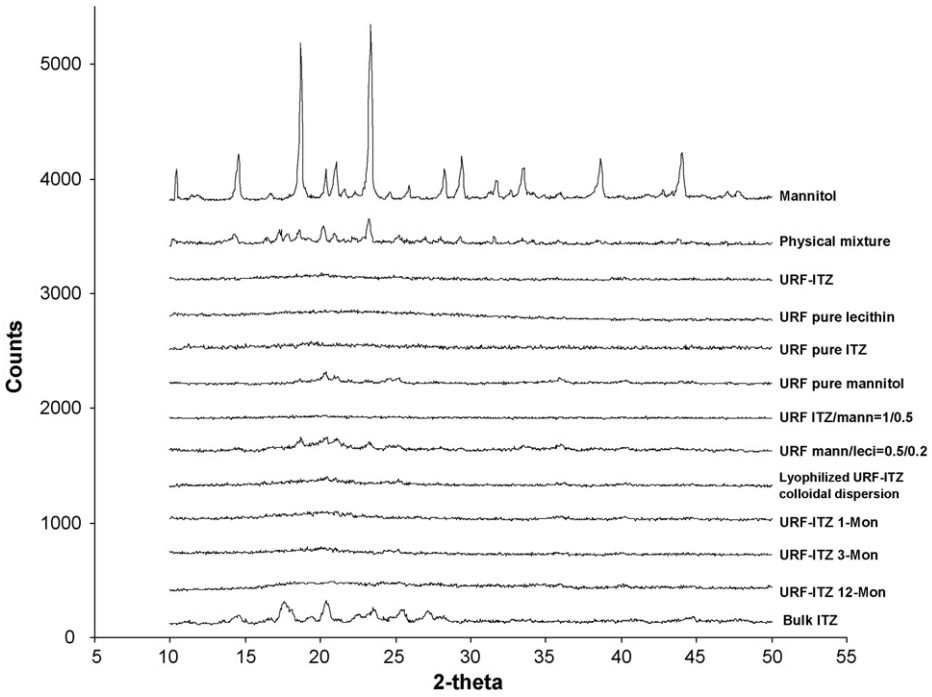

Fig. 1. X-ray powder diffraction patterns (from the top to bottom): micronized bulk mannitol, physical mixture (physical mixture of ITZ:mannitol:lecithin = 1:0.5:0.2), URF-ITZ (URF processed ITZ:mannitol:lecithin = 1:0.5:0.2), URF processed lecithin, ITZ, mannitol, ITZ:mannitol = 1:0.5 (ratio in weight), mannitol:lecithin = 0.5:0.2 (ratio in weight), respectively, re-lyophilized powder from a fast frozen colloidal dispersion of the URF-ITZ (20 mg ITZ/mL) after sitting at room temperature for 15 min, URF-ITZ powders after stored in desiccators under vacuum at room temperature for 1, 3 and 12 months, respectively, micronized bulk ITZ.

showed a single T_g at 44.5 °C. The corresponding physical mixture only showed one endothermic melting peak at 166.2 °C. XRD was conducted on powders of the following compositions, and the results indicated that the URF pure ITZ (no excipients; 100% potency) was amorphous, URF pure mannitol was crystalline, URF pure lecithin was amorphous, URF ITZ:mannitol = 1:0.5 (ratio by weight) was amorphous, and URF mannitol:lecithin = 0.5:0.2 (ratio by weight) was partially crystalline (Fig. 1).

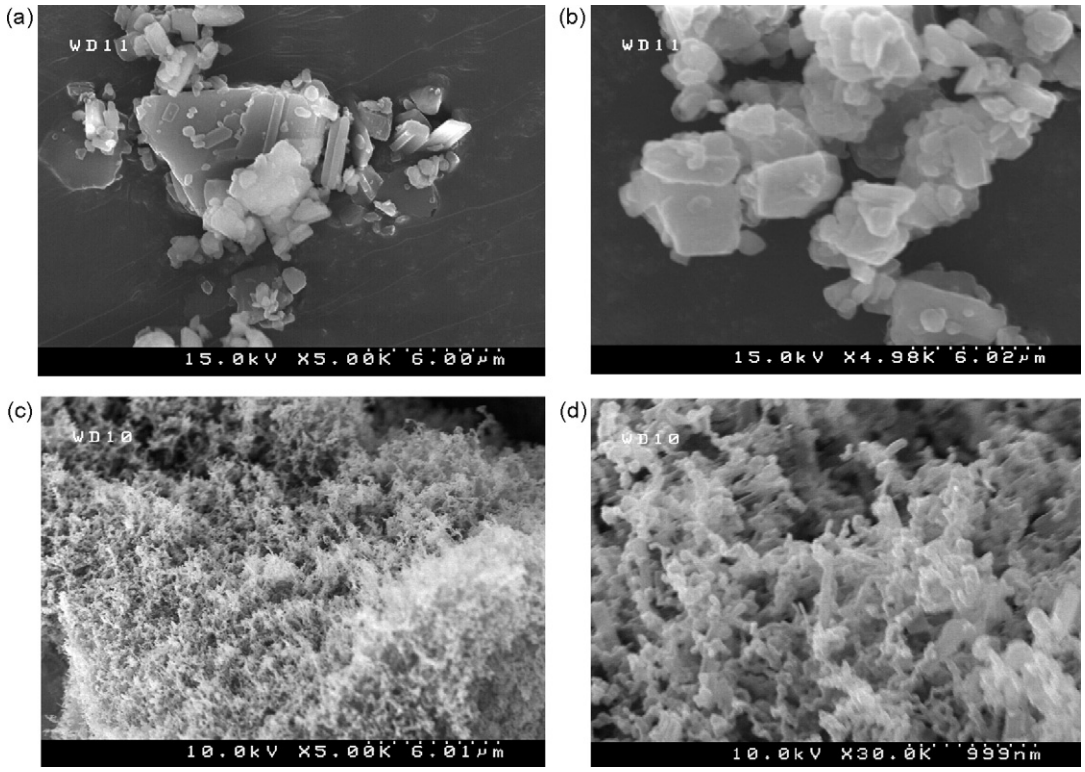

Fig. 2. SEM images of (a) bulk ITZ at a magnification of 5 k (b) physical mixture of ITZ:mannitol:lecithin = 1:0.5:0.2 at a magnification of 5 k (c) URF-ITZ (URF processed ITZ:mannitol:lecithin = 1:0.5:0.2) at a magnification of 5 k (d) URF-ITZ at a magnification of 30 k.

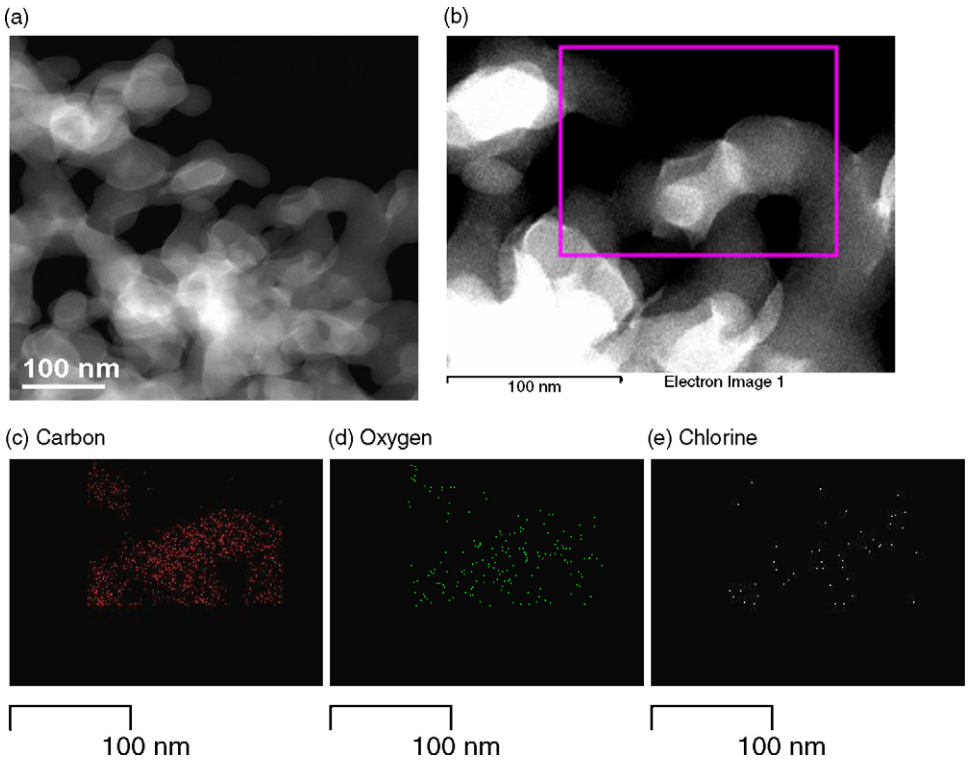

Fig. 3. (a) STEM image of nanoparticles of URF-ITZ (URF processed ITZ:mannitol:lecithin = 1:0.5:0.2). (b) STEM image of nanoparticles of URF-ITZ at a higher magnification for elemental analysis by area scan using energy dispersive spectroscopy. The particles within the pink frame were scanned for elemental distribution. (c) Carbon atoms distribution in the scanned nanoparticles. (d) Oxygen atoms distribution in the scanned nanoparticles. (e) Chlorine atoms distribution in the scanned nanoparticles.

3.4. Particle size distribution

The particle size distributions that measured by laser diffraction are shown in Table 1. The URF-ITZ powder showed a narrow size range with D_{50} and D_{90} (diameter at which the cumulative sample volume was under 50 and 90%, respectively) are less than 230 and 540 nm, respectively, compared to the corresponding values of 2.75 and 5.10 μm in the corresponding physical mixture.

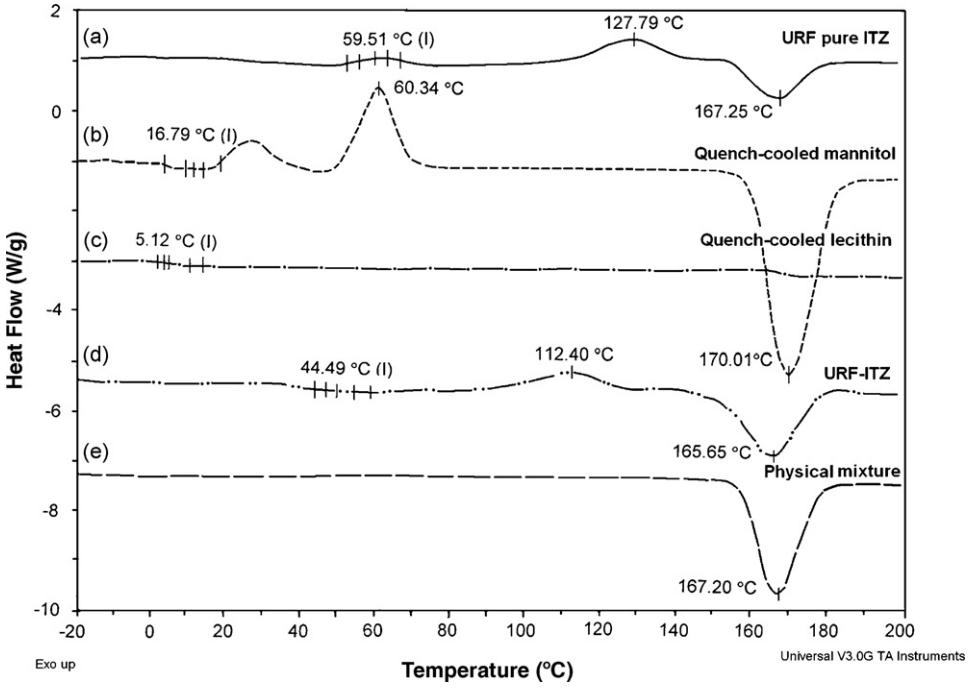

Fig. 4. DSC profiles of (a) URF processed pure ITZ, (b) quench-cooled mannitol, (c) quench-cooled lecithin, (d) URF-ITZ (ITZ:mannitol:lecithin = 1:0.5:0.2 ratio in weight), (e) physical mixture of ITZ:mannitol:lecithin = 1:0.5:0.2 ratio in weight.

Table 1
Particle size distributions and specific surface areas (SSA) of URF-ITZ (URF processed ITZ:mannitol:lecithin = 1:0.5:02) powders, physical mixture (physical mixture of ITZ:mannitol:lecithin = 1:0.5:02) and bulk ITZ

Samples	Particle size (μm)			SSA (m^2/g)
	D(v, 0.1)	*D*(v, 0.5)	*D*(v, 0.9)	
URF-ITZ	0.09	0.23	0.54	71.48
Physical mixture	1.45	2.75	5.1	1.80
Bulk ITZ	1.6	2.89	4.95	2.20

3.5. Specific surface area and true density

The specific surface area of the URF-ITZ powder was 71.48 m^2/g, in contrast to 2.20 m^2/g for the unprocessed bulk ITZ and 1.80 m^2/g for the physical mixture. The URF process rendered the ITZ/excipients about 30–40 times greater surface area as compared to that of the bulk ITZ and the physical mixture, as seen in Table 1.

True density of ITZ, mannitol and lecithin were determined to be 1.37, 1.50, 1.10 g/cm^3, respectively, by helium pycnometry.

3.6. Supersaturation dissolution study

The maximum concentration of dissolved ITZ in simulated lung fluid was determined under supersaturated conditions (100-times C_{eq}). The results are shown in Fig. 5. The C_{eq} in simulated lung fluid was about 10 ng/mL after shaking at 37 °C for 3 days with excess ITZ present. The URF-ITZ powder showed a value of the measured concentration of dissolved ITZ (C) versus C_{eq} (C/C_{eq}) of 22-times at 5 min in simulated lung fluid and the highest value of 27-times at 15 min. The supersaturated ITZ concentration gradually decreased to about 7-times at 3 h. The physical mixture demonstrated about 2-times the measured C/C_{eq} at 15 and 30 min, and gradually decreased and reached a plateau at C_{eq} value after 2 h in the simulated lung fluid. The cumulative extent of supersaturation was calculated as the area under the supersaturation curve (AUSC), which was 25,000 and 2500 ng min/mL for URF-ITZ and the corresponding physical mixture, respectively.

3.7. In vitro aerosol performance

The aerodynamic particle size of the colloidal dispersion of URF-ITZ for nebulization, with an equivalent of 100 mg ITZ in 5 mL, is summarized in Table 2. The TED was 52.97 mg out of 100 mg ITZ available for nebulization. The FPF was 66.96% with a fine particle dose (amount of aerosol droplets entering the impactor less than 4.7 μm, TED × FPF, indication of the dose delivered to the deep lung) delivered at a rate of 3.55 mg/min. The MMAD of the atomized droplets was 2.38 μm with a GSD of 2.56, which is suitable for deep lung delivery.

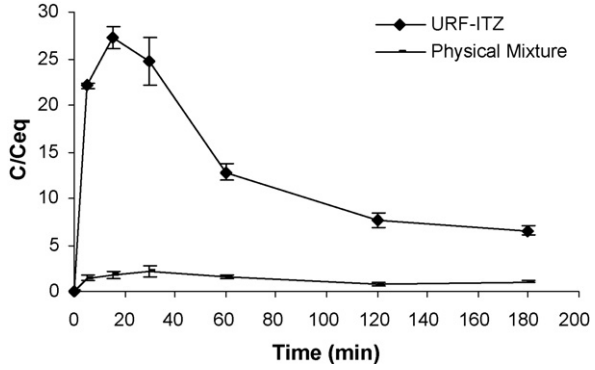

Fig. 5. Dissolution profiles of URF-ITZ (URF processed ITZ:mannitol:lecithin = 1:0.5:0.2) and physical mixture (ITZ:mannitol:lecithin = 1:0.5:0.2) in simulated lung fluid (pH 7.4) at supersaturation conditions (e.g., 100-times equilibrium solubility of crystalline ITZ was added) using 100-mL vessels and small paddle apparatus at 100 rpm and 37 °C.

Table 2
Cascade impaction data for URF-ITZ (URF processed ITZ:mannitol:lecithin = 1:0.5:02) powder, aerosolized using the Aeroneb Professional micropump nebulizer at an air flow rate of 28.3 L/min for 10 min

Total emitted dose (mg)	52.97
Fine particle fraction (%)	66.96
Fine particle dose (mg/min)	3.55
Mass median aerodynamic diameter (MMAD) (μm)	2.38
Geometric standard deviation (GSD)	2.56

3.8. Stability study

The crystallinity of the URF-ITZ powder was monitored using XRD and the results are depicted in Fig. 1. There was no characteristic crystalline peak of ITZ or mannitol detected by XRD after storage for up to 12 months, indicating the powder retained its amorphous morphology when stored at room temperature and protected from humidity.

Additionally as a simulation for the period of the URF-ITZ powder dispersion to be nebulized, the absence of characteristic crystalline peaks confirmed that the URF-ITZ in the colloidal dispersion remained amorphous over the nebulization time period.

3.9. Single-dose, 24-h pharmacokinetic study in mice

Mice inhaled the single-dose aerosols of the nebulized URF-ITZ colloidal dispersion for 10 min. ITZ concentrations versus time in the blood and lung samples of the single-dose 24-h pharmacokinetic study are presented in Fig. 6. The pharmacokinetic parameters are listed in Table 3. In the lung samples, the C_{max} was 21.19 μg/g (wet lung tissue) at 0.5 h post-dosing. The $t_{1/2}$ was 7.4 h and the $K_{elimination}$ rate constant was 0.093 h^{-1}, which may explain the ITZ lung level was maintained at 2.16 μg/g (wet lung weight) for up to 24 h. In serum, based on a one-compartmental analysis, the C_{max} was 1.64 μg/mL at 2 h after dosing. The $K_{01\ absorption}$ and $K_{10\ elimination}$ rate constants were 0.757 and 0.195 h^{-1}, respectively. The $t_{1/2\ k01}$ and $t_{1/2\ k10}$ were 0.92 and 3.55 h, respectively.

Table 3
Pharmacokinetic parameters for lung deposition and serum concentration in male outbred ICR mice (25 g) after inhalation of nebulized URF-ITZ (URF processed ITZ:mannitol:lecithin = 1:0.5:02) nanoparticles dispersion following single-dose administration

Pharmacokinetic parameter	SFL-ITZ*		URF-ITZ	
	Lung[a]	Serum[b]	Lung[a]	Serum[b]
C_{max} (μg/g)	13.4	0.12	21.19	1.64
T_{max} (h)	1	5.35	0.5	2
$t_{1/2\ K01}$ (h)		3.73		0.92
$t_{1/2\ K10}$ (h)	5.5	3.7	7.44	3.55
$K_{01\ absorption}$ (h^{-1})		0.186		0.76
$K_{10\ elimination}$ (h^{-1})	0.13	0.188	0.093	0.2
AUC_{0-24} (μg h/mL)			126.74	5.53
$AUC_{0-\infty}$ (μg h/mL)	85.8	1.69	149.94	5.60

* Data of SFL-ITZ were adapted from (Vaughn et al., 2006) for comparison purposes.

[a] Based on non-compartmental analysis of the lung tissue concentrations versus time.

[b] Calculated based on one-compartmental analysis of the serum concentrations versus time for extravascular administration.

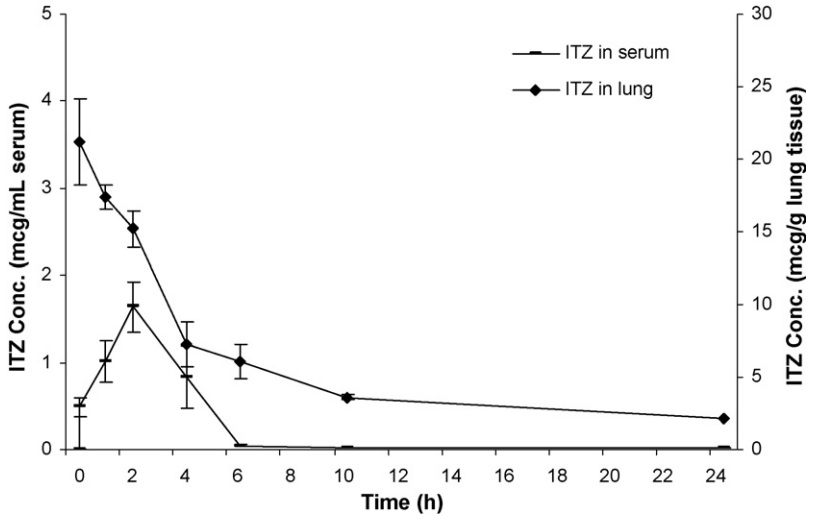

Fig. 6. Serum concentration and lung deposition of ITZ in male outbred ICR mice after inhalation of nebulized URF-ITZ (URF processed ITZ:mannitol:lecithin = 1:0.5:0.2, ratio by weight) colloidal dispersion by single-dose administration (an equivalent dose exposure of 100 mg/kg by aerosolization over a 10 min period). Data is presented as mean ± S.D.

4. Discussion

4.1. Characterization of URF-ITZ and comparison to SFL-ITZ

Pulmonary delivery of the nebulized colloidal dispersion of nanostructured aggregates of URF-ITZ dramatically improved bioavailability compared to the previously reported formulation of SFL-ITZ, more specifically a faster absorption rate, shorter T_{max}, almost double the C_{max} in lung tissue, and 10-times higher C_{max} in blood were observed (Vaughn et al., 2006). Both of the formulations were tested in the same animal model according to identical dosing apparatus and procedures. Further work would be needed to characterize the *in vitro* properties of the SFL-ITZ dispersions in order to understand these differences in bioavailability.

Both SFL and URF processes were able to create submicron particles of drug domains within a polymer matrix due to rapid freezing of a co-dissolved drug and excipient mixture (Vaughn et al., 2005; McConville et al., 2006; Overhoff et al., 2007b). Solid dispersions are systems in which drug particles are homogeneously distributed throughout a solid matrix. A solid solution results when the drug is molecularly dispersed throughout a solid matrix (Kapsi and Ayres, 2001); here, the particle size of the drug has been reduced to its absolute minimum without any crystalline drug domains (Leuner and Dressman, 2000). Solid dispersions or solid solutions of poorly water-soluble drugs have greatly enhanced extents and rates of dissolution, due to increased exposure area of drug to the dissolution media and higher Gibbs free energy of the amorphous versus crystalline states (Martin, 1993; Matteucci et al., 2007). This leads to significantly improved bioavailability, and therefore, is of interest to pharmaceutical formulation scientists.

In this study, powder XRD, MTDSC and EDS were used to differentiate between a solid dispersion and solid solution. Based on the MTDSC results, a single T_g for the URF-ITZ powder was observed between the T_gs of the amorphous pure ITZ and mannitol. The modified Gordon–Taylor equation for ternary systems (Van Den Mooter et al., 2001) was used to predict the T_g of the URF-ITZ powder:

$$T_g = \frac{w_1 T_{g1} + K_1 w_2 T_{g2} + K_2 w_3 T_{g3}}{w_1 + K_1 w_2 + K_2 w_3} \quad (1)$$

where w_1, w_2 and w_3 are the weight fractions of lecithin, mannitol and ITZ, respectively, and T_{g1}, T_{g2} and T_{g3} are the corresponding glass transition temperatures. K is a constant calculated by

$$K_1 = \frac{\rho_1 T_{g1}}{\rho_2 T_{g2},} \quad K_2 = \frac{\rho_2 T_{g2}}{\rho_3 T_{g3}} \quad (2)$$

where ρ_1, ρ_2, and ρ_3 are the corresponding true densities. The predicted T_g' of 42.3 °C, agrees closely with the measured T_g of 44.5 °C for the URF-ITZ powder.

The XRD pattern indicated that URF processed pure mannitol was partially crystalline; whereas ITZ:mannitol = 1:0.5 and ITZ:mannitol:lecithin = 1:0.5:0.2 (URF-ITZ) were completely amorphous. Absence of crystallinity of the drug or complete absence of a drug peak (either in DSC or XRD) indicates that the composition is a solid solution (Damian et al., 2000). The partial crystallization of the mannitol by URF and lyophilization may be expected from its low T_g of 16.8 °C. Kim et al. also reported similar results and difficulty in obtaining amorphous mannitol freeze-dried powder (Kim et al., 1998). ITZ may retard mannitol crystallization from the glassy state, which is expected from a miscible polymer pair. Lecithin itself is in amorphous form. Mannitol and lecithin may plasticize the extremely hydrophobic ITZ in the URF-ITZ powder leading to improved wettability, though also reduction of its T_g.

Moreover, EDS was performed to analyze the distribution of ITZ in the drug/excipient matrix by mapping elemental distributions. Theoretically, the ratios of the main elements (carbon, oxygen, chlorine) at any given area should be constant if ITZ, mannitol and lecithin formed a solid solution. EDS is capable of highly selective spatial resolution of chemistry, from volumes as small as 1 μm^3 (Sarver, 1996). The qualitative elemental distribution images suggest a generally homogenous distribution of ITZ in the scanned aggregated nanoparticles of URF-ITZ. Based on MTDSC, XRD, and EDS results, the components of the URF-ITZ composition are fully miscible and dispersed in each other at the molecular level. Thus, the URF-ITZ powder is primarily a solid solution formed by the immobilization of molecularly dispersed ITZ and excipients (mannitol, lecithin) on a timescale of milliseconds during the URF process (Engstrom et al., 2008; Overhoff et al., 2007a).

4.2. Role of the surfactant and mannitol

In the URF-ITZ composition, the soy lecithin is an accepted excipient for aerosol inhalation (http://www.accessdata.fda.gov/scripts/cder/iig/getiigWEB.cfm). It is acceptable in the lung as the biocom-

patible and biodegradable substance, i.e., phosphatidylcholine (PC) comprises an estimated 70–80% of the naturally occurring pulmonary surfactant pool (Myers et al., 1993). Besides playing an important role in improving the wettability of the nanoparticles containing ITZ, it may also enhance the absorption of ITZ in the lung epithelium. Phospholipids are known to penetrate cell membranes, decrease bilayer stability, and thereby induce changes in the cytoskeleton that can affect tight junctions and accelerate paracellular passage of drugs (Ott et al., 1981; Roelofsen et al., 1989; Lindmark et al., 1998). Codrons et al. (2004) reported that incorporation of DPPC into a dry powder formulation of parathyroid hormone for pulmonary administration produced a high systemic bioavailability of 34% in rats. DPPC has also been shown to increase absorption of insulin via pulmonary delivery and enhance the hypoglycemic effect on rats relative to free insulin, when formulated as an admixture or in liposomes (Liu et al., 1993; Mitra et al., 2001). The addition of very small amounts of exogenous DPPC may transiently alter local PC concentrations (Bernhard et al., 1997), and/or accelerate the surfactant turnover process, leading to enhanced penetration of the drug molecules through the lung alveolar cells into the systemic circulation (Liu et al., 1993).

In the present study, the high systemic absorption of ITZ following pulmonary dosing may be attributed partially to the inhaled exogenous PC, as well as the small particle size. The PC from lecithin may facilitate both dissolution and permeation, via dilated pulmonary epithelial tight junctions. Thus, the selection of lecithin as an excipient in the URF-ITZ composition offers the potential of marked improvement in absorption, without adding toxicity to the formulation. Moreover, the presence of the surfactant in the ITZ nanoparticle formulations is important to stabilize the dispersion and aid in wetting upon deposition in the lungs. Nanoparticles have high surface energies, due to the high surface-to-volume ratio and tend to agglomerate. Wettability of the URF-ITZ powder is critical for forming dispersions in the aqueous medium prior to nebulization. Mannitol was chosen as the second excipient in the URF-ITZ composition, to improve wetting of the URF-ITZ powder by introducing water into the matrix to aid dissolution.

Once the drug is deposited in the aqueous lining fluid in the lung, the mannitol may quickly dissolve, resulting in a porous drug matrix. Lecithin will initially swell, causing stress relaxation of the matrix and allowing water ingress before it dissolves. These processes will help stabilize the ITZ from aggregation and precipitation during dissolution.

The URF process dramatically increased the surface area of the nanostructured aggregates of URF-ITZ to about 40 times that of the corresponding physical mixture for dissolution. Additionally, the thinner diffusion boundary layer for the smaller particle size raises the dissolution rate (Tinke et al., 2005; Crisp et al., 2007). Furthermore, the degree of crystallization of undissolved ITZ in the particles upon exposure to the lung fluid is reduced by the rapid dissolution of the high surface area nanoparticles relative to microparticles, as examined in detail elsewhere (Matteucci et al., 2007). A combination of increased intrinsic solubility and reduced chance to crystallize of undissolved ITZ in the media may provide an explanation for the URF-ITZ to produce supersaturation values more than 20-times C_{eq} in simulated lung fluid.

4.3. Deposition of the nanoparticles containing ITZ

It is generally accepted that aerosol droplets with aerodynamic diameters between 1 and 5 μm can be delivered into the alveolar lumen after inhalation (Byron and Phillips, 1990). Furthermore, the aerosol diameter of aqueous droplets produced by nebulizers may readily be tuned to this optimal size range (Courrier et al., 2002). Nanoparticles may be distributed more uniformly throughout the nebulized droplets than microparticles (Chan and Gonda, 1988; Rabinow, 2004). For instance, if the volume fraction, f, of particles in the solvent is 0.01, then only about 1/100 of 3 μm carrier droplets will contain a 3 μm particle. In contrast each carrier droplet would contain about twenty-two 230 nm particles according to the relationship:

$$\frac{N_{\text{particles}}}{N_{\text{drops}}} = f\frac{r_{\text{drop}}^3}{r_{\text{particle}}^3} \tag{3}$$

Thus, the rate of drug absorption may be increased for nanoparticle relative to microparticle colloidal dispersions, by promoting more uniform drug distribution throughout the alveoli (Jacobs and Muller, 2002; Ostrander et al., 1999). More specifically, for a 32.5 μg drug/g lung dose (chosen based on the ITZ C_{max} recovered from lung tissue at $t = 0.5$ h and the corresponding blood concentration given in Fig. 6) delivered as 3 μm drug particles, only 1 in 75 alveoli are estimated to receive a particle. However, approximately 30 drug particles are deposited in each alveolus when the same dose is delivered as 230 nm drug particles.

4.4. Absorption of ITZ as a function of the composition and particle morphology

A drug in an amorphous state will possess a higher intrinsic solubility than in its crystalline state (Chiou, 1977; Yamashita et al., 2003; Van Drooge et al., 2004; Matteucci et al., 2007). The URF-ITZ powder was shown to be an amorphous solid solution by DSC, XRD, and elemental mapping analysis. Furthermore, the exposure of ITZ molecules to the dissolution medium is maximized in the high surface area particles, as the soluble mannitol and lecithin dissolve in the lung lining fluid. The dispersed ITZ molecules are then available as free molecules to form a supersaturated solution (Leuner and Dressman, 2000). After deposition of the inhaled ITZ nanoparticles in the lung lining fluid, the rate and extent of dissolution influence the permeation rate of ITZ through the lung epithelium to reach systemic circulation.

The effects of particle size, dissolution rate, extent of supersaturation and permeability on absorption of poorly water-soluble drugs in the lungs were examined with a model reported recently (Tam et al., 2008). The Noyes–Whitney equation describes the dissolution rate of ITZ spherical nanoparticles. The permeate concentration was assumed to be zero as the drug concentration in the blood may be assumed to be insignificant compared to that in the alveolar fluid and thus the permeation is irreversible (Patton and Byron, 2007). The thickness of the human alveolar membrane (100–200 nm) is small versus the diameter of the alveolus (300 μm) (Patton, 1996; Courrier et al., 2002) and thus planar coordinates are appropriate. Consider a material balance on the fluid surrounding a drug particle in the alveolar fluid as shown in Fig. 7. The accumulation of dissolved drug in the fluid of a single alveolus C is given by the inlet flow from particle dissolution and the depletion by an outlet flow from drug permeation through the epithelium (Tam et al., 2008)

$$\frac{\partial C}{\partial t} = N_{\text{p}} D\frac{2\pi r}{V}(C_{\text{sat}} - C) - \frac{AP}{V}C \tag{4}$$

where N_{p} is the number of drug particles deposited in each alveolus, D is the diffusion coefficient of the drug, P is the permeability, and V and A are the volume and surface area, respectively, of an annular layer of lung fluid in a single alveolus adjacent to the epithelium (Fig. 7). Absorption half-lives were determined as the time when $M_{\text{permeated}}/M_0 = 0.5$ or likewise, $r^3/r_0^3 = 0.5$. It is instructive to consider the two boundary conditions for absorption: purely dissolution limited and purely permeation-limited. For

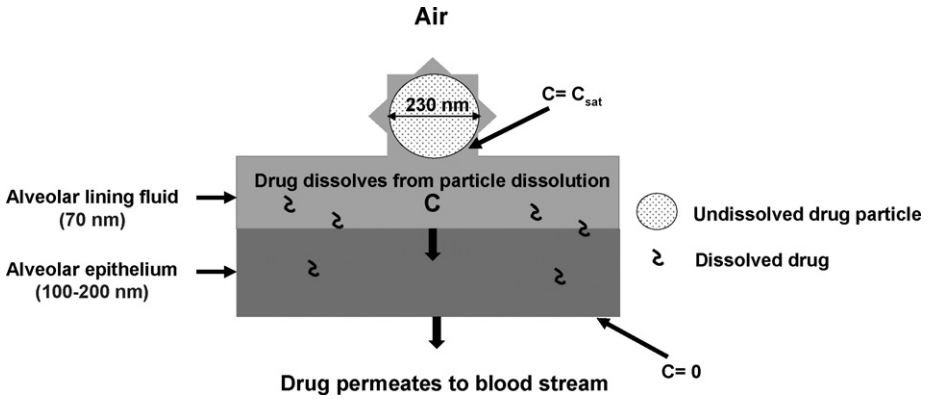

Fig. 7. Schematic of material balance used in dissolution/permeation model. The concentration of dissolved drug in the alveolar fluid of a single alveolus, C, is given by the inlet flow from particle dissolution and the depletion by an outlet flow from drug permeation through the epithelium.

purely dissolution limited absorption ($P = \infty$ and $C \to 0$), the absorption half-life becomes

$$t_{50} \approx \frac{0.37 r_0^2}{DC_{sat}} \rho \quad (5)$$

and for purely permeation-limited absorption (dissolution rate $\to \infty$ and $C = C_{sat}$)

$$t_{50} = \frac{0.5 M_0}{A_{Alv} P C_{sat}} \quad (6)$$

where $A_{Alv} = A$ for planar geometry.

The Wilke–Chang equation was used to estimate a $D = 5.26 \times 10^{-6}$ cm^2/s (Mccabe et al., 2001) for ITZ. A P value of 5.61×10^{-5} cm/s was chosen based on experimental ITZ permeabilities in intestinal membranes (Varma et al., 2005). Common permeabilities of poorly water-soluble drugs with similar molecular sizes in lung cell cultures range between 10^{-6} and 10^{-4} cm/s (Forbes and Ehrhardt, 2005). The number of drug particles deposited in the lungs was calculated from an estimated drug dose and the average particle volume. The drug dose, or the total mass of drug deposited in the lungs, was approximated to be 5.8 μg (32.5 μg/g wet lung tissue) based on the lung tissue C_{max} (21.2 μg/g) and the corresponding blood concentration (492 ng/mL) from the single-dose pharmacokinetic study. The number of alveoli in a mouse was estimated to be $\sim 2.25 \times 10^7$, calculated using an alveolar surface area of 680 cm^2 (Geelhaar and Weibel, 1971) and alveolus diameter of 31 μm (Lum and Mitzner, 1987) for mice. Total alveolar fluid volume was estimated to be 8.3 μL, based on a human alveolar surface fluid volume of 15 mL (Niven, 1992; Patton, 1996) and the ratio of human lung to mouse lung weight.

Fig. 8 shows the predicted absorption half-lives for particles ranging from 50 nm to 3 μm in diameter for a wide equilibrium solubility range, from 10 ng/mL to 10 μg/mL. Particle sizes between 50 and 230 nm are representative of URF-ITZ particles, as determined by STEM images (Fig. 3a) and light scattering results (Table 1), whereas a particle size of 3 μm is typical of particles traditionally delivered to the lungs (Courrier et al., 2002). The t_{50} for a crystalline 3 μm ITZ particle (C_{sat} = 10 ng/mL) was estimated to be 200 h (Fig. 8G), far too slow to be appropriate for therapy. In contrast, t_{50} values for the amorphous 230 nm particles were only 14.7 min, which would be consistent with the kinetics for the studies with mice in Fig. 6.

The t_{50} values are shown for purely dissolution limited absorption (diamonds, infinite permeability) and purely permeation-limited absorption (asterisks, $C = C_{sat}$). For permeation-limited absorption, t_{50} does not change with particle size for the 50 and 230 nm particles as predicted from Eq. (6). However, it is much larger for a 3 μm particle deposited in an alveolus because of the larger M_0. Based on *in vivo* lung and blood levels, only 1 in 67 alveoli would be estimated to receive a 3 μm drug particle compared to about 30 particles per alveolus for a 230 nm particle. For the 230 nm

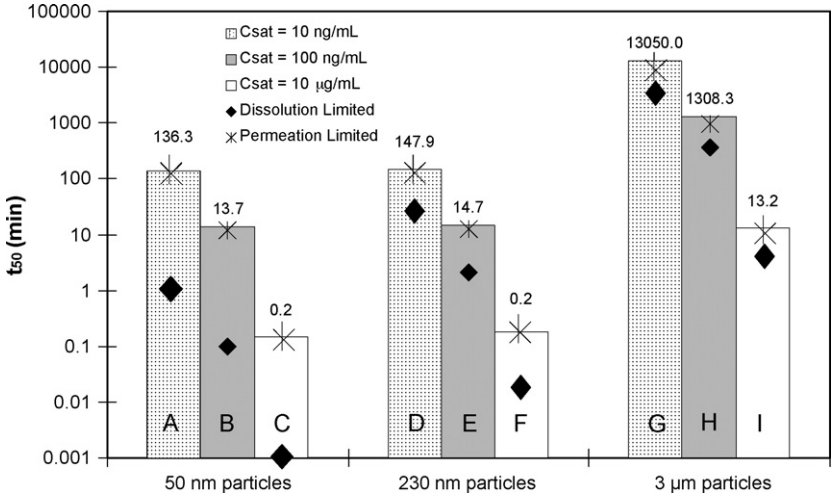

Fig. 8. Predicted absorption half-lives (time for 50% of drug to dissolve and permeate through lung epithelium) for various particle sizes and solubilities. The values are also shown for purely dissolution limited absorption (diamonds, infinite permeability) and purely permeation-limited absorption (asterisks, $C = C_{sat}$).

particles, the smaller M_0 resulting from the more uniform distribution of particles throughout all of the alveoli is a major benefit, as it produces smaller t_{50} values relative to microparticles.

For all three C_{sat} values with 3 μm particles, the absorption rate is strongly limited by the dissolution rate as expected for a BCS Class II drug. Thus, the t_{50} decreases orders of magnitude with an increase in C_{sat} by 1000-fold, which increases the driving force for particle dissolution. Interestingly, the absorption became much more permeability limited than dissolution rate limited for the 230 nm particles, no longer exhibiting BCS Class II behavior, for all three C_{sat} values. For the high surface area 50 nm particles, the dissolution rate limited t_{50} was about two orders of magnitude shorter than the permeation-limited value. With the extremely rapid dissolution rates relative to permeation, absorption times remained fairly constant versus particle diameter for sub-230 nm particles, at a given equilibrium solubility (Fig. 8A–F).

Despite the high dissolution rate for the 230 nm crystalline particles, the t_{50} value was still undesirably long because of the effect of the low C_{sat} on the permeability. The t_{50} was reduced markedly by an increase in C_{sat} for the amorphous URF-ITZ. Yet a further improvement in permeation rates may be achieved by incorporating permeability enhancers. In fact, the increased systemic absorption rate of URF-ITZ over SFL-ITZ (Vaughn et al., 2006), despite the similar particle sizes, may be explained by the incorporation of lecithin in the URF-ITZ formulation, a known permeation enhancer. As a result, an order of magnitude increase in C_{max} was achieved in circulation (URF-ITZ: 1.64 μg/mL serum versus SFL-ITZ: 0.12 μg/mL) in a shorter time (T_{max} of URF-ITZ: 2 h versus SFL-ITZ: 5.35 h) as well as a higher absorption rate of ITZ from lung to blood compared to the SFL-ITZ formulation (URF–ITZ: 0.757 h^{-1} versus SFL–ITZ: 0.186 h^{-1}) (McConville et al., 2006).

5. Conclusions

Amorphous ITZ particles were made by the ultra-rapid freezing process with FDA approved biodegradable and biocompatible excipients to achieve a mean diameter of 230 nm, a large surface area of 71 m^2/g, and a wettable surface. The particles dissolved rapidly in simulated lung fluid to produce supersaturation levels up to 27-times of C_{eq} for the crystalline form. Nebulized aqueous colloidal dispersions of the ITZ nanoparticles exhibited aerodynamic characteristics suitable for deep lung delivery. An *in vivo* single-dose 24-h pharmacokinetics study of the nebulized ITZ nanoparticle dispersion demonstrated substantial lung deposition and systemic absorption with blood levels reaching a peak of 1.6 μg/mL serum in 2 h.

To investigate the mechanism of drug absorption in the alveolar epithelium, a dissolution/permeation model was used to elucidate the effects of particle size and solubility. ITZ microparticles (3 μm) exhibited BCS Class II behavior for poorly soluble drugs with high permeabilities, where the absorption was influenced strongly by the dissolution rate. However, for 230 nm particles, the dissolution became sufficiently fast such that the concentration in the alveolar fluid reached saturation, and consequently, the absorption became permeation-limited. Therefore, a microparticle formulation with BCS Class II behavior, may exhibit a completely different kind of behavior when reformulated at the nanoscale.

Four strategies were used to raise the bioavailability. The aqueous nebulized droplets were optimized to deposit the drug in the deep lungs. The decrease in particle size (increase in surface area) enhanced the dissolution rate as well as the uniformity of the distribution of drug dose among the alveoli. The increase in C_{sat} with the formation of an amorphous polymorph, raised the driving force for permeation through the alveolar membrane. The fourth and final approach was to raise the membrane flux with lecithin, a known permeation enhancer. For the permeation-limited absorption of the 50–230 nm URF-ITZ nanoparticles, the presence of lecithin may have contributed to the enhanced systemic levels observed in the *in vivo* results. Pulmonary delivery of the ITZ nanoparticle aerosols offers the potential to treat invasive fungal infections more effectively in patient populations that have poor prognosis.

Acknowledgements

The authors are grateful to Dr. Troy Purvis for his help with HPLC analysis. This material is based upon work supported in part by the STC Program of the National Science Foundation under Agreement No. CHE-9876674, the Welch Foundation, and the Process Science and Technology Center of the University of Texas.

References

Adje, A.L., Gupta, P.K., 1997. Inhalation delivery of therapeutic peptides and proteins. In: Mahmoud, A.A.F. (Ed.), Parasitic Lung Diseases. Marcel Rcel Dekker Inc., New York, pp. 89–125.
Amidon, G.L., Lennernas, H., Shah, V.P., Crison, J.R., 1995. A theoretical basis for a biopharmaceutic drug classification: the correlation of in vitro drug product dissolution and in vivo bioavailability. Pharm. Res. 12, 413–420.
Barone, J.A., Koh, J.G., Bierman, R.H., Colaizzi, J.L., Swanson, K.A., Gaffar, M.C., Moskovitz, B.L., Mechlinski, W., Vandevelde, V., 1993. Food interaction and steady-state pharmacokinetics of itraconazole capsules in healthy male-volunteers. Antimicrob. Agents Chemother. 37, 778–784.
Bernhard, W., Haagsman, H.P., Tschernig, T., Poets, C.F., Postle, A.D., Vaneijk, M.E., Vonderhardt, H., 1997. Conductive airway surfactant: surface-tension function, biochemical composition, and possible alveolar origin. Am. J. Respir. Cell Mol. Biol. 17, 41–50.
Betageri, G.V., Makarla, K.R., 1995. Enhancement of dissolution of glyburide by solid dispersion and lyophilization techniques. Int. J. Pharm. 126, 155–160.
Bosquillon, C., Lombry, C., Preat, V., Vanbever, R., 2001. Influence of formulation excipients and physical characteristics of inhalation dry powders on their aerosolization performance. J. Control. Release 70, 329–339.
Byron, P., Phillips, E., 1990. In: Byron, P.R. (Ed.), Absorption, Clearance and Dissolution in the Lung. Respiratory Drug Delivery CRC, Boca Raton, FL, pp. 107–141.
Chan, H.K., Gonda, I., 1988. Development of a systematic theory of suspension inhalation aerosols. 2. Aggregates of monodisperse particles nebulized in polydisperse droplets. Int. J. Pharm. 41, 147–157.
Chiou, W.L., 1977. Pharmaceutical applications of solid dispersion systems: X-ray diffraction and aqueous solubility studies on griseofulvin-polyethylene glycol 6000 systems. J. Pharm. Sci. 66, 989–991.
Chow, A.H.L., Tong, H.H.Y., Chattopadhyay, P., Shekunov, B.Y., 2007. Particle engineering for pulmonary drug delivery. Pharm. Res. 24, 411–437.
Clark, T.A., Hajjeh, R.A., 2002. Recent trends in the epidemiology of invasive mycoses. Curr. Opin. Infect. Dis. 15, 569–574.
Codrons, V., Vanderbist, F., Ucakar, B., Preat, V., Vanbever, R., 2004. Impact of formulation and methods of pulmonary delivery on absorption of parathyroid hormone (1–34) from rat lungs. J. Pharm. Sci. 93, 1241–1252.
Cook, R.O., Pannu, R.K., Kellaway, I.W., 2005. Novel sustained release microspheres for pulmonary drug delivery. J. Control. Release 104, 79–90.
Courrier, H.M., Butz, N., Vandamme, T.F., 2002. Pulmonary drug delivery systems: recent developments and prospects. Crit. Rev. Ther. Drug Carrier Syst. 19, 425–498.
Crisp, M.T., Tucker, C.J., Rogers, T.L., Williams, R.O., Johnston, K.P., 2007. Turbidimetric measurement and prediction of dissolution rates of poorly soluble drug nanocrystals. J. Control. Release 117, 351–359.
Damian, F., Blaton, N., Naesens, L., Balzarini, J., Kinget, R., Augustijns, P., Van Den Mooter, G., 2000. Physicochemical characterization of solid dispersions of the antiviral agent UC-781 with polyethylene glycol 6000 and Gelucire 44/14. Eur. J. Pharm. Sci. 10, 311–322.
Davies, N.M., Feddah, M.R., 2003. A novel method for assessing dissolution of aerosol inhaler products. Int. J. Pharm. 255, 175–187.
Ebbesen, M., Jensen, T.G., 2006. Nanomedicine: techniques, potentials, and ethical implications. J. Biomed. Biotechnol. 2006, 51516.
Edwards, D.A., Dunbar, C., 2002. Bioengineering of therapeutic aerosols. Annu. Rev. Biomed. Eng. 4, 93–107.
Engstrom, J.D., Lai, E.S., Ludher, B.S., Chen, B., Milner, T.E., Williams 3rd., R.O., Kitto, G.B., Johnston, K.P., 2008. Formation of stable submicron protein particles by thin film freezing. Pharm. Res. 25, 1334–1346.
Evans, J.C., Scherzer, B.D., Tocco, C.D., Kupperblatt, G.B., Becker, J.N., Wilson, D.L., Saghir, S.A., Elder, E.J., 2006. Preparation of nanostructured particles of poorly water soluble drugs via a novel ultra-rapid freezing technology. In: Svenson, S. (Ed.), Polymeric Drug Delivery–Polymeric Matrices and Drug Particle Engineering, ACS Symposium Series 924. American Chemical Society, Washington, DC, pp. 320–328.

Forbes, B., Ehrhardt, C., 2005. Human respiratory epithelial cell culture for drug delivery applications. Eur. J. Pharm. Biopharm. 60, 193–205.
Geelhaar, A., Weibel, E.R., 1971. Morphometric estimation of pulmonary diffusion capacity. 3. The effect of increased oxygen consumption in Japanese Waltzing mice. Respir. Physiol. 11, 354–366.
Goerke, J., 1998. Pulmonary surfactant: functions and molecular composition. Biochim. Biophys. Acta 1408, 79–89.
Hancock, B.C., Parks, M., 2000. What is the true solubility advantage for amorphous pharmaceuticals? Pharm. Res. 17, 397–404.
Hu, J., Johnston, K.P., Williams 3rd., R.O., 2004. Nanoparticle engineering processes for enhancing the dissolution rates of poorly water soluble drugs. Drug. Dev. Ind. Pharm. 30, 233–245.
Jacobs, C., Muller, R.H., 2002. Production and characterization of a budesonide nanosuspension for pulmonary administration. Pharm. Res. 19, 189–194.
Kapsi, S.G., Ayres, J.W., 2001. Processing factors in development of solid solution formulation of itraconazole for enhancement of drug dissolution and bioavailability. Int. J. Pharm. 229, 193–203.
Kim, A.I., Akers, M.J., Nail, S.L., 1998. The physical state of mannitol after freeze-drying: effects of mannitol concentration, freezing rate, and a noncrystallizing cosolute. J. Pharm. Sci. 87, 931–935.
Leuner, C., Dressman, J., 2000. Improving drug solubility for oral delivery using solid dispersions. Eur. J. Pharm. Biopharm. 50, 47–60.
Lin, S.J., Schranz, J., Teutsch, S.M., 2001. Aspergillosis case - fatality rate: systematic review of the literature. Clin. Infect. Dis. 32, 358–366.
Lindmark, T., Kimura, Y., Artursson, P., 1998. Absorption enhancement through intracellular regulation of tight junction permeability by medium chain fatty acids in Caco-2 cells. J. Pharmacol. Exp. Ther. 284, 362–369.
Liu, F.Y., Shao, Z., Kildsig, D.O., Mitra, A.K., 1993. Pulmonary delivery of free and liposomal insulin. Pharm. Res. 10, 228–232.
Lum, H., Mitzner, W., 1987. A species comparison of alveolar size and surface forces. J. Appl. Physiol. 62, 1865–1871.
Martin, A., 1993. Physical Pharmacy, Fourth ed. Williams &Wilkins, Baltimore.
Matteucci, M.E., Brettmann, B.K., Rogers, T.L., Elder, E.J., Williams 3rd., R.O., Johnston, K.P., 2007. Design of potent amorphous drug nanoparticles for rapid generation of highly supersaturated media. Mol. Pharm. 4, 782–793.
Mawson, S., Yates, M.Z., Oneill, M.L., Johnston, K.P., 1997. Stabilized polymer microparticles by precipitation with a compressed fluid antisolvent. 2. Poly(propylene oxide)- and poly(butylene oxide)-based copolymers. Langmuir 13, 1519–1528.
Mccabe, W.L., Smith, J.C., Harriott, P., 2001. Unit Operations of Chemical Engineering. McGraw Hill Inc., Boston, MA.
Mccallion, O.N., Taylor, K.M., Thomas, M., Taylor, A.J., 1995. Nebulization of fluids of different physicochemical properties with air-jet and ultrasonic nebulizers. Pharm. Res. 12, 1682–1688.
McConville, J.T., Williams, R.O., Carvalho, T.C., Iberg, A.N., Johnston, K.P., Talbert, R.L., Burgess, D., Peters, J.I., 2005. Design and evaluation of a restraint-free small animal inhalation dosing chamber. Drug Dev. Ind. Pharm. 31, 35–42.
McConville, J.T., Overhoff, K.A., Sinswat, P., Vaughn, J.M., Frei, B.L., Burgess, D.S., Talbert, R.L., Peters, J.I., Johnston, K.P., Williams 3rd., R.O., 2006. Targeted high lung concentrations of itraconazole using nebulized dispersions in a murine model. Pharm. Res. 23, 901–911.
Mehrad, B., Paciocco, G., Martinez, F.J., Ojo, T.C., Iannettoni, M.D., Lynch 3rd., J.P., 2001. Spectrum of Aspergillus infection in lung transplant recipients: case series and review of the literature. Chest 119, 169–175.
Mitra, R., Pezron, I., Li, Y., Mitra, A.K., 2001. Enhanced pulmonary delivery of insulin by lung lavage fluid and phospholipids. Int. J. Pharm. 217, 25–31.
Myers, M.A., Thomas, D.A., Straub, L., Soucy, D.W., Niven, R.W., Kaltenbach, M., Hood, C.I., Schreier, H., Gonzalez-Rothi, R.J., 1993. Pulmonary effects of chronic exposure to liposome aerosols in mice. Exp. Lung Res. 19, 1–19.
Niven, R.W., 1992. Pharmaceutical Inhalation Aerosol Technology. Marcel Dekker, Inc., New York.
Ostrander, K.D., Bosch, H.W., Bondanza, D.M., 1999. An in-vitro assessment of a nanocrystal beclomethasone dipropionate colloidal dispersion via ultrasonic nebulization. Eur. J. Pharm. Biopharm. 48, 207–215.
Ott, P., Hope, M.J., Verkleij, A.J., Roelofsen, B., Brodbeck, U., Van Deenen, L.L., 1981. Effect of dimyristoyl phosphatidylcholine on intact erythrocytes. Release of spectrin-free vesicles without ATP depletion. Biochim. Biophys. Acta 641, 79–87.
Overhoff, K.A., Engstrom, J.D., Chen, B., Scherzer, B.D., Milner, T.E., Johnston, K.P., Williams 3rd., R.O., 2007a. Novel ultra-rapid freezing particle engineering process for enhancement of dissolution rates of poorly water-soluble drugs. Eur. J. Pharm. Biopharm. 65, 57–67.
Overhoff, K.A., Moreno, A., Miller, D.A., Johnston, K.P., Williams 3rd., R.O., 2007b. Solid dispersions of itraconazole and enteric polymers made by ultra-rapid freezing. Int. J. Pharm. 336, 122–132.
Patton, J., 1996. Mechanisms of macromolecule absorption by the lungs. Adv. Drug Del. Rev. 19, 3–36.
Patton, J.S., Byron, P.R., 2007. Inhaling medicines: delivering drugs to the body through the lungs. Nat. Rev. Drug Discov. 6, 67–74.
Patton, J.S., Mccabe, J.G., Hansen, S.E., Daugherty, A.L., 1989. Absorption of human growth hormone from the rat lung. Biotechnol. Ther. 1, 213–228.
Peeters, J., Neeskens, P., Tollenaere, J.P., Van Remoortere, P., Brewster, M.E., 2002. Characterization of the interaction of 2-hydroxypropyl-beta-cyclodextrin with itraconazole at pH 2, 4 and 7. J. Pharm. Sci. 91, 1414–1422.
Poirier, J.M., Hardy, S., Isnard, F., Tilleul, P., Weissenburger, J., Cheymol, G., 1997. Plasma itraconazole concentrations in patients with neutropenia: advantages of a divided daily dosage regimen. Ther. Drug Monit. 19, 525–529.
Rabinow, B.E., 2004. Nanosuspensions in drug delivery. Nat. Rev. Drug Discov. 3, 785–796.
Roelofsen, B., Kuypers, F.A., Op Den Kamp, J.A., Van Deenen, L.L., 1989. Influence of phosphatidylcholine molecular species composition on stability of the erythrocyte membrane. Biochem. Soc. Trans. 17, 284–286.
Rogers, T.L., Johnston, K.P., Williams 3rd., R.O., 2001. Solution-based particle formation of pharmaceutical powders by supercritical or compressed fluid CO_2 and cryogenic spray-freezing technologies. Drug Dev. Ind. Pharm. 27, 1003–1015.
Rowland, M., Tozer, T., 1995. Absorption and disposition kinetics. In: Rowland, M., Tozer, T. (Eds.), Clinical Pharmacokinetics: Concepts and Applications, third ed. Lippincott Williams & Wilkins, Baltimore, pp. 11–52.
Sarkari, M., Brown, J., Chen, X., Swinnea, S., Williams 3rd., R.O., Johnston, K.P., 2002. Enhanced drug dissolution using evaporative precipitation into aqueous solution. Int. J. Pharm. 243, 17–31.
Sarver, L.W., 1996. SEM and EDS analyze materials. Adv. Mater. Process. 150, 19–21.
Singh, N., Husain, S., 2003. Aspergillus infections after lung transplantation: clinical differences in type of transplant and implications for management. J. Heart Lung Transplant. 22, 258–266.
Six, K., Verreck, G., Peeters, J., Augustijns, P., Kinget, R., Van Den Mooter, G., 2001. Characterization of glassy itraconazole: a comparative study of its molecular mobility below $T(g)$ with that of structural analogues using MTDSC. Int. J. Pharm. 213, 163–173.
Smith, D., Van De Velde, V., Woestenborghs, R., Gazzard, B.G., 1992. The pharmacokinetics of oral itraconazole in AIDS patients. J. Pharm. Pharmacol. 44, 618–619.
Sobel, J.D., 2000. Practice guidelines for the treatment of fungal infections. For the Mycoses Study Group. Infectious Diseases Society of America. Clin. Infect. Dis. 30, 652.
Tam, J., Mcconville, J.T., Williams 3rd., R.O., Johnston, K.P., 2008. Amorphous cyclosporin nanodispersions for enhanced pulmonary deposition and dissolution. J. Pharm. Sci., doi:10.1002/jps.21367.
Tinke, A.P., Vanhoutte, K., De Maesschalck, R., Verheyen, S., De Winter, H., 2005. A new approach in the prediction of the dissolution behavior of suspended particles by means of their particle size distribution. J. Pharm. Biomed. Anal. 39, 900–907.
Van Den Mooter, G., Wuyts, M., Blaton, N., Busson, R., Grobet, P., Augustijns, P., Kinget, R., 2001. Physical stabilisation of amorphous ketoconazole in solid dispersions with polyvinylpyrrolidone K25. Eur. J Pharm. Sci. 12, 261–269.
Van Drooge, D.J., Hinrichs, W.L., Frijlink, H.W., 2004. Anomalous dissolution behaviour of tablets prepared from sugar glass-based solid dispersions. J. Control. Release 97, 441–452.
Varma, M.V., Sateesh, K., Panchagnula, R., 2005. Functional role of P-glycoprotein in limiting intestinal absorption of drugs: contribution of passive permeability to P-glycoprotein mediated efflux transport. Mol. Pharm. 2, 12–21.
Vaughn, J.M., Gao, X., Yacaman, M.J., Johnston, K.P., Williams 3rd., R.O., 2005. Comparison of powder produced by evaporative precipitation into aqueous solution (EPAS) and spray freezing into liquid (SFL) technologies using novel Z-contrast STEM and complimentary techniques. Eur. J. Pharm. Biopharm. 60, 81–89.
Vaughn, J.M., Mcconville, J.T., Burgess, D., Peters, J.I., Johnston, K.P., Talbert, R.L., Williams 3rd., R.O., 2006. Single dose and multiple dose studies of itraconazole nanoparticles. Eur. J. Pharm. Biopharm. 63, 95–102.
Verreck, G., Six, K., Van Den Mooter, G., Baert, L., Peeters, J., Brewster, M.E., 2003. Characterization of solid dispersions of itraconazole and hydroxypropylmethylcellulose prepared by melt extrusion—Part I. Int. J. Pharm. 251, 165–174.
Yamashita, K., Nakate, T., Okimoto, K., Ohike, A., Tokunaga, Y., Ibuki, R., Higaki, K., Kimura, T., 2003. Establishment of new preparation method for solid dispersion formulation of tacrolimus. Int. J. Pharm. 267, 79–91.
Yang, W., Peters, J.I., Williams 3rd., R.O., 2008. Inhaled nanoparticles—a current review. Int. J. Pharm. 356, 239–247.